A Home-based Dual-mode Upper Limb Rehabilitation System: Teleoperation Mode and Bilateral Mode with sEMG and IMU

He Li, Student Member, *IEEE*, Shuxiang Guo, Fellow, *IEEE*, Ruijie He, Student Member, *IEEE*, Bin Wang, and Mingchao Ding

Abstract*—Upper limb hemiplegia is a common functional disorder among stroke patients, significantly affecting their quality of life. To address this issue, robot-assisted upper limb rehabilitation training has emerged as a new therapeutic approach, breaking through time and space limitations of traditional rehabilitation. Based on the above, a home-based dual-mode upper limb rehabilitation system is built, including teleoperation mode based on a cloud server and bilateral mode with fusion of Surface Electromyography (sEMG) and Inertial Measurement Unit (IMU). In the telerehabilitation mode, patients can receive professional guidance and regular training at home, greatly enhancing the accessibility of rehabilitation services. The experiments with the master side in Beijing City (China) and the slave side in three different cities are conducted through a cloud server. The slave side is controlled by the master side, and the contact force is sent back to the master side. In the bilateral mode, the intention of continuous movements across subjects can be accurately predicted via the fusion of sEMG and IMU, improving the naturalness of human-robot interaction. In the subject-independent modeling, the Root Mean Square Error (RMSE) under fusion showed a relative decrease of 15.0329% ($p < 10^{-4}$) compared to IMU data alone, and a significantly greater reduction of 61.9376% ($p < 10^{-4}$) in comparison with sEMG data alone. Robot-assisted upper limb exoskeleton, cloud-based teleoperation and bilateral training based on sEMG and IMU collectively form a new rehabilitation system, representing part of the future rehabilitation trend.

***Index Terms*—Upper limb hemiplegia, Exoskeleton-assisted rehabilitation, Cloud-based telerehabilitation, Surface Electromyography (sEMG), Inertial Measurement Unit (IMU), Force feedback**

I. Introduction

HEMIPLEGIA, a common sequela caused by brain damage such as stroke, brain trauma, or neurodegenerative diseases, seriously affects patients' physical functions and quality of life. Among these conditions, upper limb hemiplegia is particularly prominent [1], as it restricts patients' ability to perform daily activities and profoundly impacts their mental health and social participation. Due to the crucial role of upper limbs in daily life, the rehabilitation of upper limb hemiplegia has become a focus point in the medical field. With the advancement of medical technology, rehabilitation treatment is increasingly regarded as a key approach to enhancing both the quality of life and functional recovery for hemiplegic patients. Effective rehabilitation can not only help hemiplegia patients regain some or even all of their limb functions [2] but also prevent complications caused by long-term bed rest and enhance their ability to live independently. Therefore, research on the rehabilitation of upper limb hemiplegia has become particularly important.

Although traditional rehabilitation has been successful in improving functional recovery in patients with hemiplegia [3], it relies on the experience of physical therapists. And the limited human resources and limited training frequency make it difficult to provide sustained, intensive and personalized treatment. In response to these challenges, robot-assisted rehabilitation systems have gained increasing attention. Compared with traditional face-to-face rehabilitation, telerehabilitation has shown many significant advantages [11]. It breaks geographical and traffic constraints, expands service coverage, and reduces time and transportation costs. With the smart device and sensor technology, remote systems can collect and analyze data in real time, providing personalized treatment plans and instant feedback to ensure the effectiveness and adaptability of treatment. Atashzar et al. [12] built a haptics-enabled robotic neurorehabilitation system, in which the framework for neural-network-based supervised training is proposed. However, the bulky equipment is difficult to adapt to home-based settings, and the high cost makes it unaffordable for many patients and their families, thus hindering the widespread adoption of telerehabilitation technology and the maximization of

This work was supported in part by the National Natural Science Foundation of China (61703305), in part by National High-tech Research and Development Program (863 Program) of China (2015AA043202), in part by SPS KAKENHI (15K2120). (Corresponding author: Shuxiang Guo)

H. Li and R. J. He are with the School of Life Science, Beijing Institute of Technology, Beijing 100081, China, also with the Key Laboratory of Convergence Biomedical Engineering System and Healthcare Technology, The Ministry of Industry and Information Technology, Beijing Institute of Technology, Beijing 100081, China (email: {lihe, heruijie}@bit.edu.cn).

S. X. Guo is with is with the Department of Electronic and Electrical Engineering, Southern University of Science and Technology, Shenzhen, Guangdong 518055, China, and also with Aerospace Center Hospital, School of Life Science and the Key Laboratory of Convergence Medical Engineering System and Healthcare Technology, Ministry of Industry and Information Technology, Beijing Institute of Technology, Beijing 100081, China (e-mail: guo.shuxiang@sustech.edu.cn).

B. Wang and M. C. Ding are with the Department of Peripheral Vascular Intervention, Aerospace Center Hospital, School of Life Science, Beijing Institute of Technology, Beijing 100081, China (email: wangbin@asch.net.cn; dingmingchao@asch.net.cn).

practical utility. Yi Liu et al. [4] developed a telerehabilitation system for home-based training, in which enhanced therapist-patient remote interaction is considered. However, this system is limited to a local area network environment and only involves one degree of freedom (DoF) - the elbow joint. These limitations mean that the scope of application and function of the system need to be expanded, and it cannot fully meet the diversified rehabilitation needs of patients. Based on motion tracking, Jing Bai et al. [13] presented a cloud communication-based rehabilitation system for the upper limb. While virtual games can provide interactivity and fun, during the early stages of rehabilitation, patients often require more precise and personalized physical support and guidance than current systems can adequately provide. In summary, the existing telerehabilitation systems need improvement in terms of device adaptability, cost-effectiveness, functional diversity and responsiveness to patients' personalized needs. These issues limit the widespread adoption of the telerehabilitation systems and their potential in promoting upper limb rehabilitation.

Bilateral training is becoming an important component in post-stroke rehabilitation, which can guide and control the affected limb's movements by capturing signals from the healthy limb. This approach not only promotes neuroplasticity but also improves rehabilitation outcomes and patient engagement. Surface Electromyography (sEMG)-based motion intention prediction directly reflects muscle activity, which is a natural and friendly human-robot interaction method [14][15]. However, these signals are susceptible to interference and exhibit significant individual variability. Inertial Measurement Units (IMU)-based motion intention prediction offers excellent robustness and stability, but it's an indirect way to infer motion intention, potentially limiting its ability to achieve natural and smooth human-robot interaction. While sEMG is excellent for capturing muscle activity details, IMU is superior for posture and motion trajectory estimation. The combination of the two can achieve a more accurate and natural human-robot interaction in rehabilitation training, significantly improving the rehabilitation effect and patient treatment experience. Yang et al. proposed an estimation method based on a sequential progressive Gaussian filtering network to form the complementary advantage of sEMG and IMU [16]. However, this study focused on subject-dependent models and lacked validation on the corresponding robot platform. Stival et al. proposed a subject-independent regression model using sEMG and IMU features [17], but their work didn't address angle regression and provide comparative explanations. Sun et al. built a feature-based convolutional neural network-bidirectional long-short-term memory network (CNN-BiLSTM) model to predict knee joint angles [18]. In summary, although the combination of sEMG and IMU can significantly improve rehabilitation outcomes and training experiences, the existing research and technologies still face challenges and limitations related to signal stability, individual adaptability and practical application scenarios. Addressing these issues requires further research and technological advancements.

In this study, a home-based dual-mode upper limb rehabilitation system is proposed, including a teleoperation mode based on a cloud platform and a bilateral mode with the fusion of sEMG and IMU. In the telerehabilitation training, with the assistance of one cloud server, therapists can remotely control the exoskeleton to drive the movements of patients' affected limb and receive force feedback from the robot-assisted side. This enables therapists to perceive the interaction force between the affected limb and the exoskeleton, allowing them to adjust the rehabilitation intensity accordingly. In the bilateral mode, by capturing both the sEMG signals generated by muscle activity and monitoring the IMU angles of limb movements, a more accurate interpretation of patients' motion intention is realized, enhancing the naturalness and precision of human-robot interaction. Through these two rehabilitation modes, regular therapist-in-the-loop telerehabilitation and home-based self-rehabilitation are facilitated. Therapist-guided telerehabilitation can provide professional advice for patients' home-based self-rehabilitation, thereby improving the overall effectiveness of bilateral rehabilitation. To sum up, the main contributions of this study are as follows:

(1) Home-based Tele-rehabilitation System: A home-based upper limb rehabilitation system utilizing force feedback teleoperation has been developed, enabling patients to receive professional guidance and perform regular training at home. This significantly enhances the accessibility and flexibility of rehabilitation services.
(2) Enhanced Prediction Accuracy of Motion Intention: In the bilateral training mode, the intention of continuous movements is accurately predicted by fusing sEMG and IMU signals, significantly improving the accuracy and naturalness of human-robot interaction.

The rest of the paper is organized as follows. Section II introduces the upper limb rehabilitation exoskeleton platform. Section III describes the dual-mode upper limb rehabilitation system, including the telerehabilitation mode and the bilateral mode via a two-branch CNN network utilizing sEMG and IMU. Section IV presents the results and discussion. Finally, Section V concludes this study.

II. Portable Upper Limb Rehabilitation Exoskeleton

Fig. 1 shows the upper limb exoskeleton worn by a subject, which includes three passive DOFs for the shoulder (abduction/adduction, internal rotation/external rotation, flexion/extension) and three active DOFs (elbow flexion/extension, wrist flexion/extension and wrist internal/external rotation). The mechanical structure mainly consists of four parts: the shoulder part, the upper arm part, the forearm part, and the wrist part. The shoulder part comprises a shoulder back plate and a junction plate. The shoulder back plate is attached to the body using two fabric straps. The junction plate is connected through a hinge to

This article has been accepted for publication in IEEE Journal of Biomedical and Health Informatics. This is the author's version which has not been fully edited and content may change prior to final publication. Citation information: DOI 10.1109/JBHI.2025.3588404

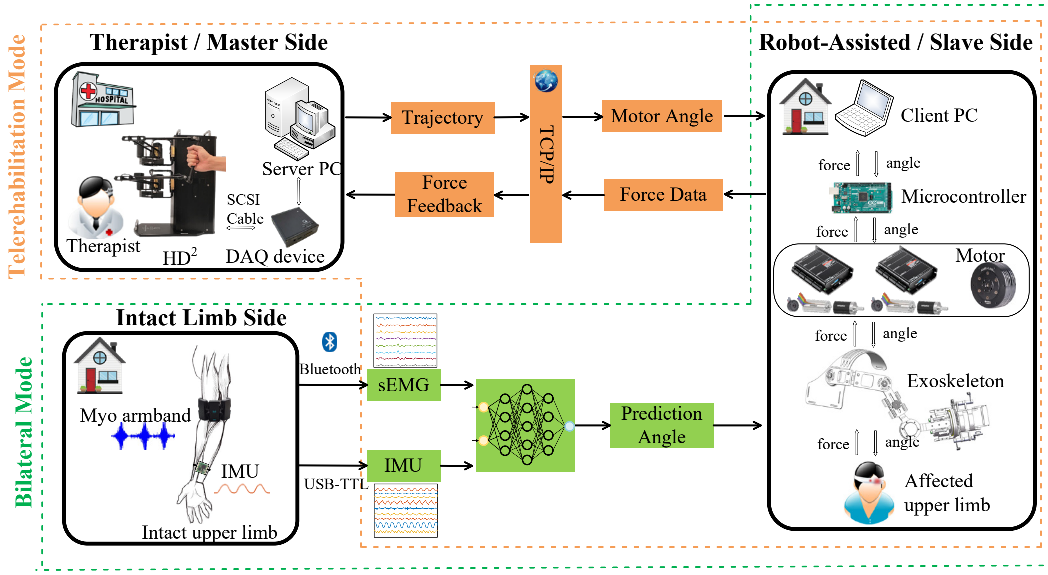

Fig. 3. The overview framework of the dual-mode system based on the telerehabilitation and the bilateral rehabilitation.

provide an additional DOF at the shoulder joint. The length of the upper and the forearm part can be adjusted to accommodate the different arm lengths among subjects. The upper arm of the exoskeleton is immobilized with a rehabilitation shoulder pad (Aiwecare, Taiwan, China), ensuring stability and comfort during use. The wrist part includes two active DOFs (wrist flexion/extension and wrist internal/external rotation).

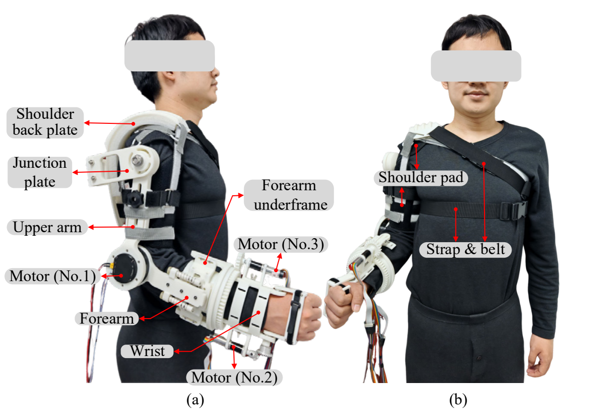

Fig. 1. The upper limb exoskeleton worn by one subject. (a) lateral view (b) front view.

The elbow rotation is achieved through a joint motor (AK 60-6, CubeMars, China). The wrist flexion/extension and internal/external rotation are each controlled by separate brushless motors (EC 16, Maxon, China). The Maxon motors are coupled with planetary gearheads (GP 16, Maxon, China) and incremental encoders (MR M-512, Maxon, China). The ESCON servo controller (Maxon, China) allows direct control of Maxon motors via Arduino using a 3-pin interface: Pulse Width Modulation (PWM), Clockwise (CW) and Counter Clockwise (CCW). The control of the exoskeleton is executed through an Arduino, which collects the angle data from IMUs. Through Inter-Integrated Circuit (IIC) communication, multiple IMUs are connected to the Arduino. For each motor, the real-time control is based on an outer position and an inner velocity loop. Fig. 2 presents a block diagram illustrating the control architecture for the multi-DOF upper-limb exoskeleton system. The system is divided into three main sections, each corresponding to a different DoF of the rehabilitation exoskeleton.

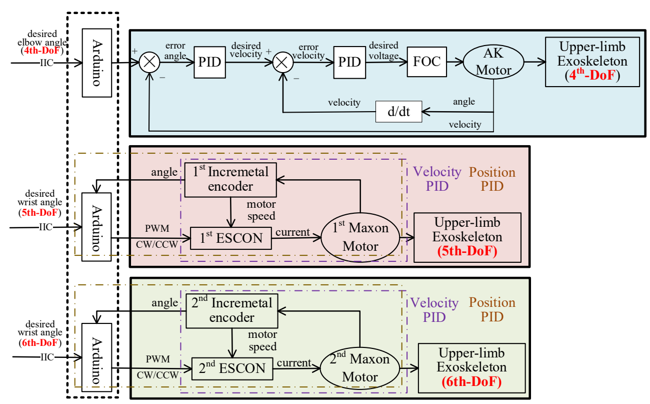

Fig. 2. The overall design of the embedded system of the upper limb rehabilitation exoskeleton.

III. Home-Based Dual-Mode Rehabilitation System Based on the Upper Limb Exoskeleton

Fig. 3 provides an overview of the dual-mode rehabilitation system, which integrates teleoperation and bilateral training. This proposed system comprises three components: the therapist side, the robot-assisted limb side and the intact limb side. The therapist side and the robot-assisted limb side together form the therapist-in-the-loop telerehabilitation mode. Meanwhile, the intact limb side and the robot-assisted limb side form the bilateral mode. In both rehabilitation modes, the upper limb exoskeleton serves as the hardware platform for the affected limb side of patients.

A. Telerehabilitation Mode

This section introduces the telerehabilitation mode, in which one subject (as a therapist) manipulates the HD^2 Haptic Device (Quanser, Canada) to deliver rehabilitation treatment to another subject (as a patient) wearing the exoskeleton (as shown in Fig. 4). The therapist can simultaneously perceive the interaction force between the patient's affected limb and the exoskeleton. In this study, the way of combining Alibaba Cloud Elastic Compute Service (ECS) example and Fast Reverse Proxy (FRP) tool is used to enable secure access from an internal network (Intranet) service to an external network (Internet). The system architecture consists of two main components: the ECS instance deployed on Alibaba Cloud as a public network proxy server, and the client device situated within the user's local network. The FRP tool is used to establish a secure channel between the two devices so that the services on the Intranet can be accessed through public IP addresses and specific ports. When conducting multi-location remote experiments, ensure the consistency of cloud server configurations.

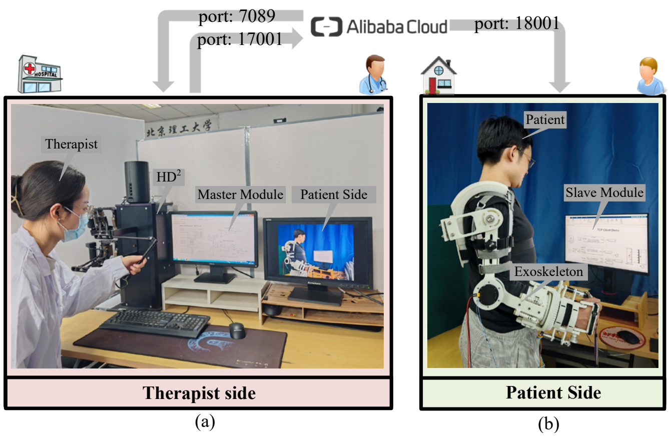

Fig. 4. The experimental setup. (a) master side (b) slave side.

The teleoperation involves controlling the three active DoFs. (elbow flexion/extension, wrist flexion/extension and wrist internal/external rotation). Fig. 5 illustrates the corresponding DoF mapping relationship between the master side (therapist side) and the slave side (patient side). A direct mapping is adopted between the master and slave angles. This means that the angle value of each DoF of the master device directly corresponds to the angle value of the corresponding DoF of the slave device, as shown in (1)-(3).

$$\theta_{s\_4^{th}\,DoF} = \theta_{m\_4^{th}\,DoF} \tag{1}$$

$$\theta_{s\_5^{th}\,DoF} = \theta_{m\_5^{th}\,DoF} \tag{2}$$

$$\theta_{s\_6^{th}\,DoF} = \theta_{m\_6^{th}\,DoF} \tag{3}$$

Where, $\theta_{m\_4^{th}\,DoF}$, $\theta_{m\_5^{th}\,DoF}$ and $\theta_{m\_6^{th}\,DoF}$ represents the angles of elbow flexion/extension, wrist flexion/extension and wrist internal/external rotation in the master side, $\theta_{s\_4^{th}\,DoF}$, $\theta_{s\_5^{th}\,DoF}$ and $\theta_{s\_6^{th}\,DoF}$ represents the angles of elbow flexion/extension, wrist flexion/extension and wrist internal/external rotation in the slave side.

The primary reasons for choosing direct mapping include the following aspects: (1) Intuitiveness and Ease of Use: Direct mapping ensures a one-to-one correspondence between the angle values of the master device and the slave device. Therapists can precisely control the movements of the device on the patient side by adjusting their actions without needing additional conversion or calculation. (2) Precision and Accuracy: In telerehabilitation training, the accurate replication of movements is crucial. Direct mapping ensures that every subtle movement of the master device is accurately reflected in the slave device without any errors. (3) Real-time Performance and Responsiveness: Direct mapping facilitates real-time synchronization between the master device and slave device, reducing delay and response time.

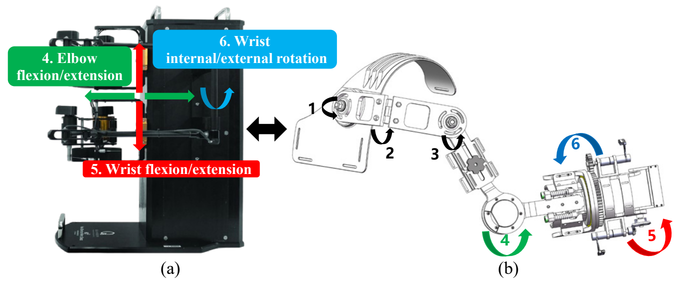

Fig. 5. The master device and slave device and their DoF mapping. (a) HD^2 (b) Solidworks model of the exoskeleton.

The operating environment of HD^2 is developed in MATLAB/Simulink using QuaRC real-time software. QuaRC is fully compatible with MATLAB and supports hardware-in-the-loop simulations. Therefore, the telerehabilitation system involved in this study is also based on this operating environment.

During the rehabilitation training process, any loss of motion or force information can lead to incorrect guidance, potentially affecting the rehabilitation effectiveness and possibly causing harm. Therefore, ensuring the accuracy and reliability of data is particularly crucial in tele-rehabilitation systems. Given this, Transmission Control Protocol (TCP) is preferred over User Datagram Protocol (UDP) for its stable and reliable transmission capabilities. Although TCP may introduce slightly higher latency, this trade-off is justified by the reduced risk of data loss or disorder. By prioritizing transmission reliability, TCP ensures that motion and force feedback during the rehabilitation process are accurately and correctly conveyed, thereby providing patients with a safer and more effective rehabilitation environment. To further enhance communication security, two methods are employed: Secure Shell (SSH) tunneling and Transport Layer Security (TLS) encryption, which provide robust protection from different perspectives. SSH tunneling is employed to create an encrypted communication channel, and TLS encryption is used to further secure data against interception during transmission.

B. Bilateral Mode via a Two-branch CNN Network Utilizing sEMG and IMU

1) Dataset

This study involves 10 subjects (labelled as Subject No.1-

This article has been accepted for publication in IEEE Journal of Biomedical and Health Informatics. This is the author's version which has not been fully edited and content may change prior to final publication. Citation information: DOI 10.1109/JBHI.2025.3588404

No.10), including 7 males and 3 females, with an average age of 24.30±2.20. All participants are right-handed and free of skeletal and neurological diseases. This research is approved by the Institutional Review Board (IRB) of Southern University of Science and Technology (Ref. No. 20240374 from January 2025). All subjects provided informed consent to participate in this study. All experimental procedures follow the Declaration of Helsinki on Medical Research involving Human Subjects.

Fig. 6 illustrates the data acquisition setup. The sEMG data is acquired through the Myo armband (Thalmic Labs, Canada), which is worn on the left upper limb. The signal sample frequency of the Myo armband is 200 Hz. The IMU data is acquired through the JY901 (Witmotion, China), which is mounted on the left forearm. It adopts a Kalman dynamic filtering algorithm, enabling the rapid determination of the module's current real-time motion attitude. The signal sample frequency of the IMU is 20 Hz. For joint angle acquisition, the Mars visual capture camera (NOKOV, China) is used, which acquires the motion characteristics of the upper limb at a sampling frequency of 200 Hz. Each volunteer performed continuous elbow joint movements for 60 s per time, with a total of five times. After each collection, the volunteers returned to a relaxed state. To avoid muscle fatigue affecting the quality of collected signals, the volunteers take a rest for about one minute after each collection.

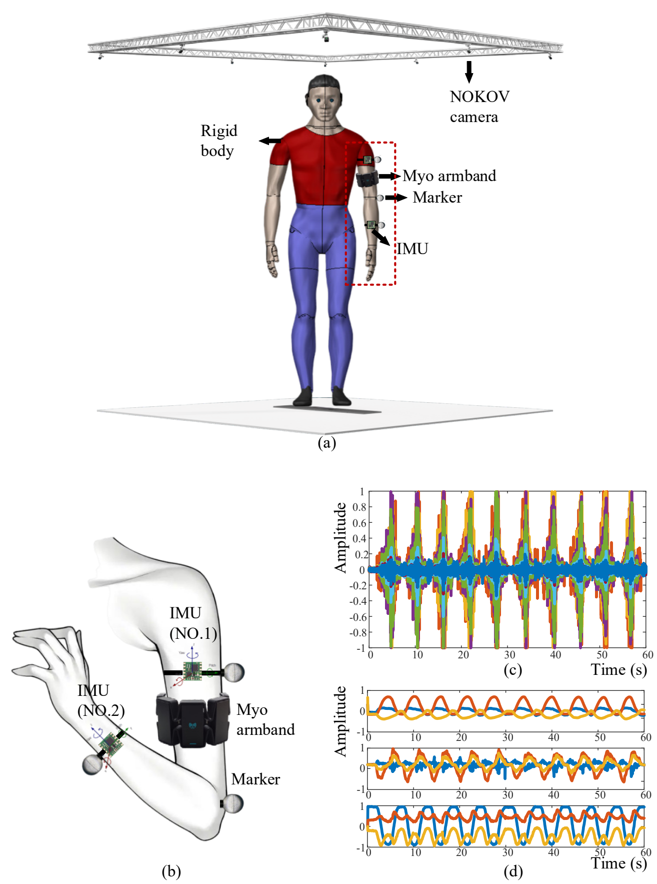

Fig. 6. Data acquisition. (a) overall acquisition diagram (b) upper arm with sEMG, IMU and marker (c) sEMG signal (d) IMU signal

2) Signal Processing

Since raw sEMG signals are often interfered by noise, data processing is necessary. The high-pass filter at 20 Hz is used to eliminate the low-frequency noise. Due to the highly non-stationary nature of sEMG signals, a sliding window approach is adopted to maintain signal stability. Fig. 7 illustrates the schematic diagram of the time window segmentation process. The sliding window has a length of 250 ms with an overlap of 200 ms, which meets the real-time control requirement of less than 300 ms. The visual capture signals and IMU signals are also segmented into windows of 250 ms with an overlap of 200 ms. The signal is processed according to the above window-adding method. The number of sliding windows for each subject at each time of experiments can be calculated according to (4).

$$N_{win} = \frac{1}{L_{add}}(N_{sam} - L_{win} + L_{add}) \tag{4}$$

Where, N_{win}, N_{sam}, L_{win}, L_{add} represents the number of sliding windows, the number of sampling points, the window length and the window increment for each subject at each time of experiments.

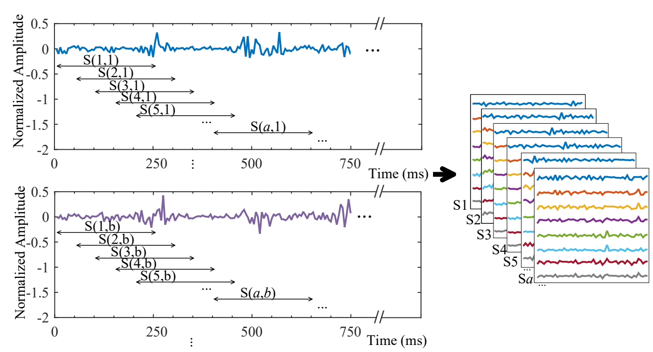

Fig. 7. The conversion of sEMG signals to sEMG images via the overlapping sliding window. S(a,b) represents the a^{th} segment of the sEMG signal from the b^{th} channel. Sa represents the a^{th} segment of sEMG signals from all 8 channels.

3) Network Architecture

This section describes the bilateral mode via a two-branch CNN network utilizing sEMG and IMU data. Unlike traditional shallow neural networks that rely on manually extracted features, a deep neural network can transform the feature representation into a new feature space via layer-by-layer feature transformation. CNN is adopted to realize the feature extraction and estimation of continuous motion intention. The output of the convolution layer is shown in (5).

$$h_i = f(w_i * x_i + b_i) \tag{5}$$

Where, x_i denotes the input of the convolution layer, h_i is the ith output feature map, w_i is the weight matrix, b_i is the bias vector, and $f(\cdot)$ represents the activation function. The rectified linear unit (ReLU) function is chosen as the activation function. The formula of ReLU can be expressed as (6).

$$h_i = f(c_i) = \max(0, c_i) \tag{6}$$

Where, c_i are the results of convolutional operations.

Compared with ordinary single-input networks, the dual-input network can process two kinds of input data, combining the respective advantages of sEMG and IMU signals. The core challenge in designing a multi-input CNN architecture is effectively integrating multiple input features for accurate prediction. Common strategies include: early fusion, late fusion and hybrid fusion:

(1) Early fusion: This approach integrates multiple input data at the early stage of the network. It is straightforward and can fully utilize the complementary information between different modal data. However, it may face the problems of scale differences between different modal data and feature redundancy.

(2) Late fusion: This method uses independent CNNs to extract features from each input data stream, then fuses these output features of each CNN at a later stage, such as the fully connected layer, through simple concatenation or averaging. This approach can flexibly handle different modal data and avoid the negative effects that may occur in the early fusion. However, it may not fully utilize the interaction between different modal data.

(3) Hybrid fusion: This approach combines the advantages of both early fusion and late fusion by fusing at various network levels. It requires careful design based on specific application scenarios and data characteristics, offering high flexibility but increasing complexity. In this study, the late fusion is adopted for the dual-input CNN model.

For sEMG signals (x_{sEMG}) and IMU signals (x_{IMU}), feature extraction is carried out by CNN respectively, and the feature representations of f_{sEMG} and f_{IMU} are obtained, as shown in (7) and (8).

$$f_{sEMG} = CNN(x_{sEMG}) \tag{7}$$

$$f_{IMU} = CNN(x_{IMU}) \tag{8}$$

Then, the two kinds of input features are combined (as shown in (9)), and the final prediction result y is obtained through the full connection layer (as shown in (10)).

$$f_{fusion} = Concatenate(f_{sEMG}, f_{IMU}) \tag{9}$$

$$y = Dense(f_{fusion}) \tag{10}$$

The structure of the dual-input and single-output CNN is shown in Fig. 8. The dual inputs are sEMG images with a size of 50*8 and IMU images with a size of 5*9, and the output is motion angles. For network training parameters, the Adam optimization algorithm is employed. It incorporates an adaptive learning rate adjustment mechanism, aiming at promoting rapid convergence and effectively handling complex high-dimensional data spaces. Specific settings include a maximum of 150 epochs, with each batch containing 128 samples. This configuration ensures computational efficiency and enhances model performance. The initial learning rate is set to 0.001. To prevent potential gradient explosion issues during training, a gradient clipping strategy with a threshold of 1 is implemented. These parameter choices and optimization settings ensure that the model can achieve efficient learning while maintaining good generalization capability.

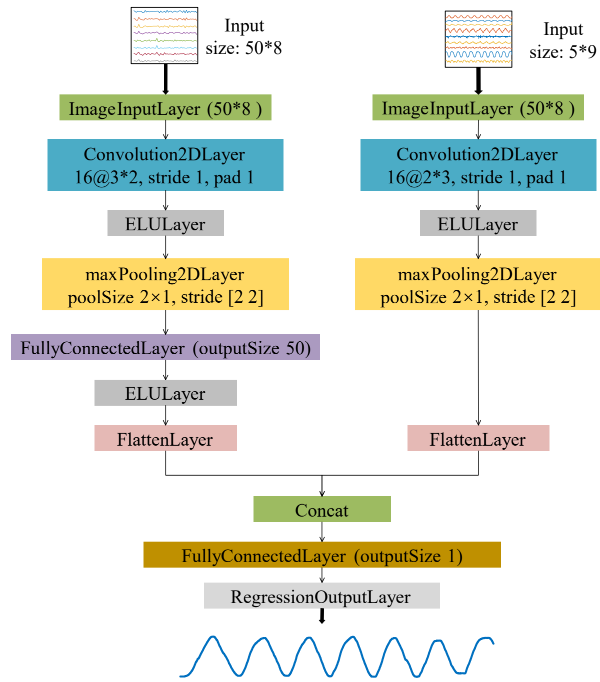

Fig. 8. The layer illustration of the dual-input CNN model.

4) Evaluation criteria

To quantitatively evaluate the prediction error, Root Mean Square Error (RMSE), Mean Absolute Error (MAE) and Correlation of Coefficient (R) are adopted. RMSE (as shown in (11)) is the standard deviation between the prediction and actual angles. RMSE is more sensitive to larger errors and effectively highlights those prediction results that significantly deviate from actual outcomes. MAE (as shown in (12)) is the average of all absolute errors between the prediction and actual angles. MAE directly reflects the average discrepancy between the predicted and actual values, and it is not influenced by extreme values, making it particularly useful for assessing the overall prediction accuracy of models. R (as shown in (13)) is a value between -1 and 1 that indicates the correlation between the prediction and actual angles. While R does not directly indicate the magnitude of prediction errors, it evaluates the model's fitting effectiveness from a different perspective, providing insight into how well the model captures the underlying trends and patterns in the data.

$$RMSE = \sqrt{\frac{1}{N}\sum_{i=1}^{N}(y_i - x_i)^2} \tag{11}$$

$$MAE = \frac{1}{N}\sum_{i=1}^{N}| y_i - x_i | \tag{12}$$

$$R = \frac{\sum_{i=1}^{N}(x_i - \bar{x})(y_i - \bar{y})}{\sqrt{\sum_{i=1}^{N}(x_i - \bar{x})^2 \sum_{i=1}^{N}(y_i - \bar{y})^2}} \tag{13}$$

Where x_i represents the prediction angles at the ith data point, $\bar{x}$ is the average value, y_i means the actual angles (visual capture angles) at the ith data point, $\bar{y}$ is the average value, and N is the total number of data points.

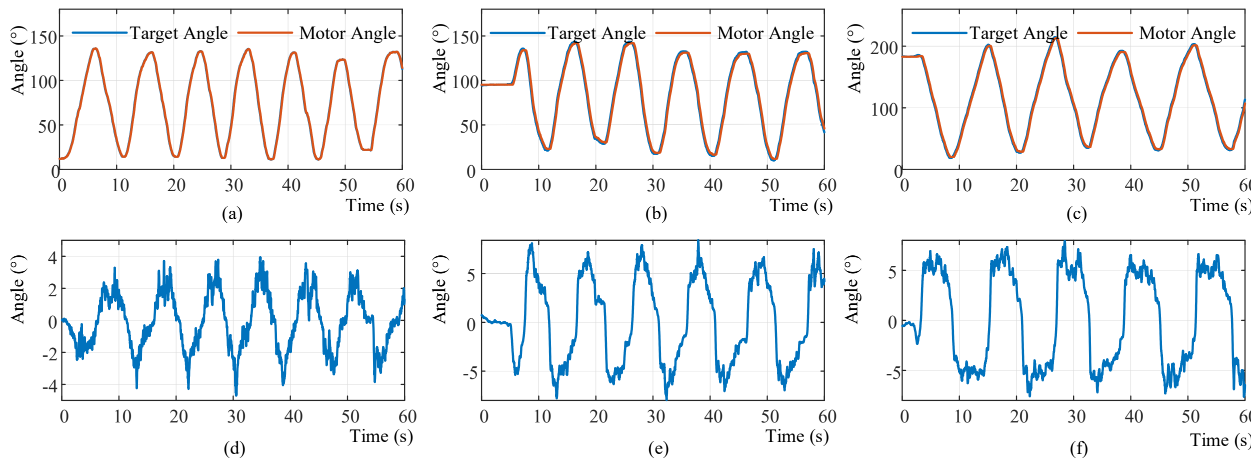

Fig. 9. The testing results of the upper limb exoskeleton. (a) motion angles of the 4th DoF (b) motion angles of the 5th DoF (c) motion angles of the 6th DoF (d) error angles of the 4th DoF (e) error angles of the 5th DoF (f) error angles of the 6th DoF.

Additionally, a one-way ANOVA is conducted to assess the statistical difference obtained by different models. The level of statistical significance is set to $p < 0.05$.

Further, to calculate the delay between IMU angles and motor angles, cross-correlation is adopted. For IMU angles ($x(n)$) and motor angles ($y(n)$), where n=0, 1, ..., $N-1$ represents the sample index and N is the signal length. Firstly, the cross-correlation function ($R_{xy}(\tau)$, where τ is the delay parameter) between $x(n)$ and $y(n)$ is calculated, as shown in (14). Then, the delay $\hat{\tau}$ that maximizes the cross-correlation function $R_{xy}(\tau)$ is identified, as shown in (15).

$$R_{xy}(\tau) = \sum_{n=0}^{N-1-\tau} x(n+\tau) \cdot y(n) \tag{14}$$

Note that when τ is negative, it indicates that x lags behind y; when τ is positive, it indicates that x leads y.

$$\hat{\tau} = \arg\max_{\tau} R_{xy}(\tau) \tag{15}$$

IV. Experimental Results

A. The Performance of the Upper Limb Exoskeleton

Bilateral training based on IMU is conducted using the 3-DoF upper limb rehabilitation exoskeleton. An IMU is worn on the healthy limb side, then it captures the movements of the healthy side and subsequently controls the exoskeleton to drive the motion of the affected limb side.

Firstly, the stability of the upper limb rehabilitation exoskeleton is tested through repeated trials. The movements of the exoskeleton are recorded to evaluate whether it operated normally, i.e., whether it followed the expected trajectory. Three groups of experiments are conducted, with 10 trials in each group. No failures are observed across all tests, indicating that the exoskeleton operates safely and stably. Secondly, the motion trajectory of the exoskeleton is recorded and analyzed. The master side refers to the patient's unaffected limb, on which the IMU is mounted. The IMU captures the motion data from the master side, which is then used to control the exoskeleton and drive the affected side to perform corresponding movements. Fig. 9 shows the motion angles and error distribution obtained from IMU-based testing.

According to (14) and (15), the control delay of the three DOFs is calculated, resulting in approximately 0 ms, 150 ms and 150 ms, respectively.

B. The Evaluation of the Telerehabilitation System

In the telerehabilitation system, communication delay and control delay are key factors that affect the treatment outcomes and patient experience. The telerehabilitation system is designed to connect medical professionals with patients via the internet, enabling patients to receive professional rehabilitation guidance and services at home or in other non-medical settings. To ensure the effectiveness and security of such systems, it is crucial to evaluate both communication latency (that is, the time required for data to travel from the sending side to the receiving side) and control latency (the time interval between the issuance and execution of an instruction).

1) Communication delay

To evaluate the effectiveness of the telerehabilitation platform, a remote experiment is conducted. The master side of the experiment is set up in Beijing (China), while the slave side is located in three different regions: Beijing (China), Shenzhen (China) and Takamatsu (Japan). In the experiment, an operator who acted as a therapist manipulates the handle of the HD^2 haptic device to generate motion signals. These signals are transmitted in real time via a cloud server to the slave side, which is used to control the movements of the exoskeleton-assisted limb. At the same time, the contact force data between the patient's affected limb and the rehabilitation exoskeleton is also transmitted back to the master side in real time, allowing the therapist to perceive the interaction process instantly. The experiment is conducted between 7:00 a.m. and 8:00 p.m. (Beijing Time), covering the major daytime activity periods. For each slave location, five repetitions of the experiment are conducted per hour to ensure data diversity and reliability. Each experiment lasted 50 s, which is sufficient to capture stable motion patterns and contact force

This article has been accepted for publication in IEEE Journal of Biomedical and Health Informatics. This is the author's version which has not been fully edited and content may change prior to final publication. Citation information: DOI 10.1109/JBHI.2025.3588404

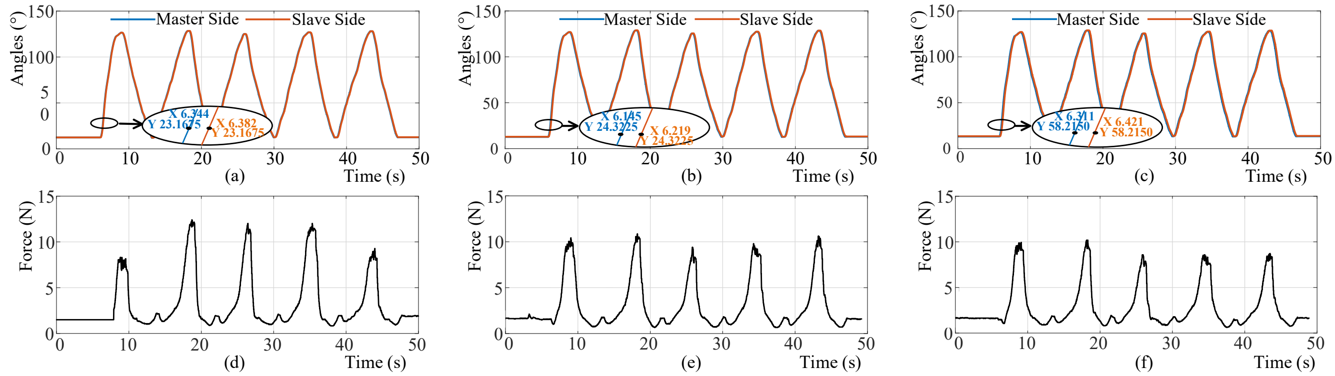

Fig. 10. Motion angles and contact force of master side (in Beijing City) and slave side (a)(d) slave side in Beijing City (b)(e) slave side in Shenzhen City (c)(f) slave side in Takamatsu City.

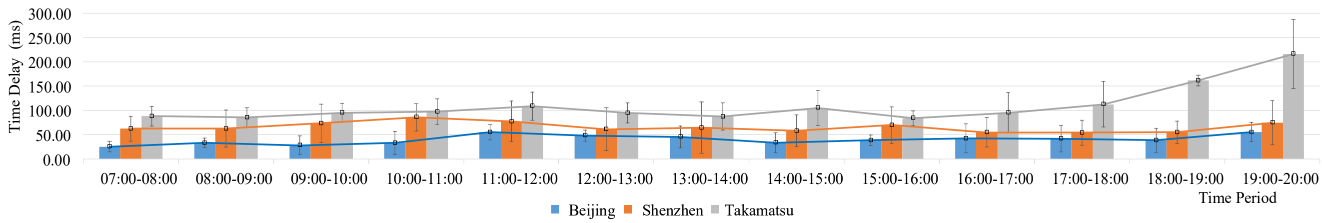

Fig. 11. Histogram of average delay of data transmission between master side and slave side.

variations while avoiding data redundancy due to excessive duration. All motion signals and contact force data generated during the experiments are recorded in detail for subsequent analysis.

With the telerehabilitation platform, therapists can provide direct kinesthetic guidance to stroke patients. A fixed motion trajectory is set on the master side to ensure consistent experimental conditions, and then a more accurate and intuitive assessment of differences in communication delays across various scenarios is determined. This approach eliminates the variability caused by changes in movement trajectory, improves the reliability of delay time measurements, and facilitates an in-depth analysis of the factors influencing the data transmission efficiency in the telerehabilitation system. Fig. 10(a)-(c) presents the motion trajectory over time, with the slave side located in Beijing, Shenzhen and Takamatsu, respectively. The motion trajectory exhibits periodic fluctuations, indicating that the patient is undergoing repetitive rehabilitation training. The therapist is also able to perceive the contact force during the training process. Fig. 10(d)-(f) illustrates the relationship between motion angles and contact force during a rehabilitation process using the exoskeleton. Both motion angles and contact force exhibit periodic fluctuations, which are characteristic of repetitive rehabilitation movements. There is a clear correlation between the peaks and troughs of motion angles and contact force. When the motion angle reaches its peak, the contact force also tends to be at its maximum. The timing of the peaks and troughs in both signals is closely aligned, indicating that the exoskeleton is effectively tracking and responding to the patient's movements.

Fig. 11 presents the hourly average communication delay (average value, AVE) and its standard deviation (STD), from 7:00 a.m. to 8:00 p.m. (Beijing Time). The bar chart with error lines clearly illustrates the communication delays and their variability across different locations. The blue, orange, and gray bars represent the communication delays in Beijing (China), Shenzhen (China), and Takamatsu (Japan), respectively. For Beijing (blue), the communication latency is generally low, with short error bars indicating low variability. For Shenzhen (orange), the communication delay is moderate, with correspondingly moderate error bars and variability. For Takamatsu (gray), in some cases, the communication delay is high, as reflected by longer error bars and greater variability.

TABLE I
THE TIME DELAY OF DATA TRANSMISSION BETWEEN THE MASTER SIDE AND THE SLAVE SIDE

	Time Delay (ms)		
	Beijing	Shenzhen	Takamatsu
MIN	25.20	53.80	83.60
MAX	54.80	85.60	215.80
Ave	38.43	66.45	109.80

For a quantitative analysis of the communication delay between the master side and slave side, the minimum, maximum and average value are calculated. As recorded in Table I, when the slave side is in Beijing, the maximum time delay is 54.80 ms, the minimum is 25.20 ms, and the average is 38.43 ms. When the slave side is in Shenzhen, the maximum time delay is 85.60 ms, the minimum is 53.80 ms, and the average is 66.45 ms. When the slave side is in Takamatsu, the maximum time delay is 215.80 ms, the minimum is 83.60 ms, and the average is 109.80 ms. The time delay increases significantly after 6 p.m. Regardless of the slave side's location, the communication delay meets the requirements, remaining below 300 ms.

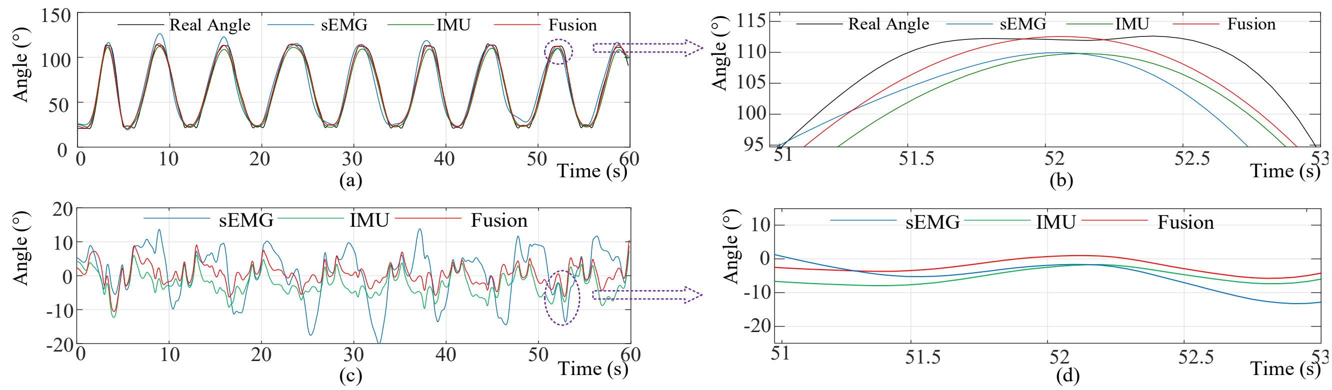

Fig 13. Angle estimation result and error curve. (a) result of angle estimation (b) partial zoom of the results of angle estimation (c) error of angle estimation (d) partial zoom of the error of angle estimation.

2) Control delay

This section analyzes the control delay of the slave motor. Fig. 12 shows the motion angles between the client PC and the microcontroller. The blue line represents the client signal received from the master PC, the red line represents the client signal received from the microcontroller, and the orange line represents the motor angle recorded by the client PC. Both the total delay (including motor control and serial transmission) and serial transmission delay are recorded. Thus, the delay of motion control can be calculated, as shown in Table II.

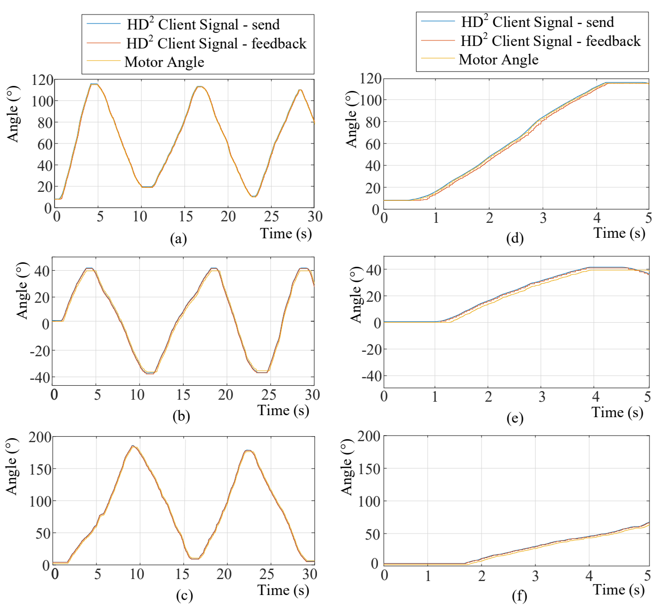

Fig. 12. Motion angles between Client PC and microcontroller (a) motion angles of the 4th DoF (b) motion angles of the 5th DoF (c) motion angles of the 6th DoF (d) partial zoom of the 4th DoF € partial zoom of the 5th DoF (f) partial zoom of the 6th DoF

TABLE II
THE TIME DELAY BETWEEN THE CLIENT PC AND MICROCONTROLLER

	Delay of motor control and serial transmission (ms)	Delay of serial transmission (ms)	Delay of motor control (ms)
4th DoF	138	16	122
5th DoF	266	17	249
6th DoF	226	17	209

This approach enables accurate isolation and quantification of delays across different components of the communication chain, thereby providing a foundation for optimizing the control system.

C. The Results and Evaluation of the Two-branch CNN Network

In this section, the proposed dual-input CNN model is presented and discussed. To evaluate the effect of the model in suppressing intra-subject and inter-subject variability during the continuous motion of the elbow joint, comparisons are made between the prediction results of the user-dependent scenario and the user-independent scenario. Both the user-dependent and user-independent models are evaluated using five-fold cross-validation.

In the user-specific (user-dependent) scenario, individual models are trained and evaluated using each user's own data. Specifically, the data from each subject is divided into five subsets, in which four subsets are used for training, and another subset is used for testing. This process is repeated five iterations, with a different subset selected as the test set in each iteration, while the remaining four subsets form the training set. Ultimately, the model's performance is evaluated based on the average result across all five iterations. This approach reduces bias due to data partitioning and provides a more stable performance estimation. Fig. 13 shows the angle estimation results and error curves based on sEMG, IMU and the fused signal. Table III summarizes the estimation results for the user-dependent scenario, where five subject-dependent models are obtained.

Additionally, one-way ANOVA is used to assess the statistical difference among different models in the user-specific scenario. The RMSE between the estimation angles based on the fusion model and the reference (vision-based) measurement is 4.1577°, indicating that the estimation error is relatively small. The RMSE of the fusion model are respectively significantly less than that of the sEMG model (11.9726°, $p < 10^{-4}$) and the IMU model (4.7902°, $p < 10^{-4}$). Compared to the IMU and sEMG models alone, the fusion model achieved RMSE reductions of 12.98% and 66.43%, respectively. These results demonstrate that the fusion

This article has been accepted for publication in IEEE Journal of Biomedical and Health Informatics. This is the author's version which has not been fully edited and content may change prior to final publication. Citation information: DOI 10.1109/JBHI.2025.3588404

TABLE III
THE ESTIMATION RESULTS FOR THE USER-DEPENDENT SITUATION

Person No.	Indicator	sEMG		IMU		sEMG+IMU	
		ave	std	ave	std	ave	std
S1	RMSE (°)	13.1445	1.7712	7.4185	0.1935	6.6583	0.2034
	MAE (°)	9.3399	1.2575	5.8645	0.2692	5.0953	0.2154
	R	0.9586	0.0065	0.9860	0.0024	0.9880	0.0012
S2	RMSE (°)	12.6922	1.4535	3.3365	0.2775	2.6635	0.2951
	MAE (°)	9.4286	1.4278	2.6129	0.3202	2.0358	0.2211
	R	0.9351	0.0103	0.997	0.0009	0.9971	0.0005
S3	RMSE (°)	9.8607	1.9426	3.6694	0.6218	3.1789	0.4529
	MAE (°)	7.2343	1.4703	2.9328	0.4446	2.5089	0.4181
	R	0.9622	0.0117	0.9958	0.0023	0.9968	0.0007
S4	RMSE (°)	11.2462	1.4689	4.8573	0.6608	4.3236	0.8472
	MAE (°)	7.8934	0.9330	3.6293	0.3707	3.1609	0.5960
	R	0.9503	0.0123	0.9916	0.0024	0.9941	0.0024
S5	RMSE (°)	14.5642	2.2624	4.4465	0.8738	3.8241	0.5861
	MAE (°)	10.1878	1.5482	3.4551	0.6239	2.8668	0.4429
	R	0.9460	0.0201	0.9958	0.0013	0.9971	0.0007
S6	RMSE (°)	13.7985	1.6521	6.5485	0.2321	5.3218	0.2456
	MAE (°)	9.2354	1.4571	4.9847	0.2587	4.2158	0.2451
	R	0.9596	0.0059	0.9897	0.0021	0.9890	0.0011
S7	RMSE (°)	12.1545	1.5415	4.6514	0.6487	4.1258	0.7985
	MAE (°)	8.1247	0.8691	3.8974	0.3745	3.2578	0.5781
	R	0.9498	0.0098	0.9845	0.0036	0.9924	0.0025
S8	RMSE (°)	10.2454	1.5641	4.1254	0.8941	3.6984	0.5614
	MAE (°)	8.4154	1.4545	3.2581	0.5784	2.9687	0.5012
	R	0.9562	0.0089	0.9921	0.0016	0.9958	0.0009
S9	RMSE (°)	10.4545	1.4541	3.9544	0.5641	3.5684	0.5681
	MAE (°)	8.5012	1.6894	3.4512	0.4685	3.0124	0.3687
	R	0.9687	0.0045	0.9899	0.0054	0.9987	0.0013
S10	RMSE (°)	11.5654	1.5689	4.8944	0.5671	4.2145	0.8911
	MAE (°)	8.0245	0.9815	3.8451	0.4512	3.1628	0.5741
	R	0.9609	0.0204	0.9909	0.0050	0.9934	0.0012
Ave	RMSE (°)	**11.9726**	**1.6679**	**4.7902**	**0.5534**	**4.1577**	**0.5449**
	MAE (°)	**8.6385**	**1.3088**	**3.7931**	**0.4160**	**3.2285**	**0.4161**
	R	**0.9547**	**0.0110**	**0.9913**	**0.0027**	**0.9942**	**0.0013**

TABLE IV
THE ESTIMATION RESULTS FOR THE USER-INDEPENDENT SITUATION

Indicator	sEMG		IMU		sEMG+IMU	
	ave	std	ave	std	ave	std
RMSE (°)	14.9586	1.8925	6.5897	1.3587	5.2478	1.5984
MAE (°)	11.3585	1.6358	5.2478	0.8225	4.5897	1.3248
R	0.9328	0.0203	0.9868	0.0061	0.9931	0.0030

strategy significantly enhances prediction accuracy in the user-dependent scenario.

In the user-independent scenario, the data partitioning strategy differs from that used in the user-dependent situation. Specifically, the datasets from the five different users are combined into a single comprehensive dataset. The following procedure is then implemented: in each iteration, data from four users is selected as the training set, and the data from the remaining one user serves as the test set. This process is repeated five times so that each user's data is used as the test set exactly once. Table IV presents the estimation results in the user-independent scenario. Additionally, one-way ANOVA is also used to assess the statistical difference of different models in the user-independent scenario. The RMSE between the estimation angles based on the fusion model and the reference (vision-based) measurement is 5.2478 °, indicating that the estimation error remains relatively small. The RMSE of the fusion model are respectively significantly less than that of the sEMG model (14.9586°, $p < 10^{-4}$) and the IMU model (6.5897°, $p < 10^{-4}$). Compared to the IMU and sEMG models alone, the fusion model achieved RMSE reductions of 15.03% and 61.94%, respectively. These results demonstrate that the fusion model significantly enhances prediction accuracy in the user-independent case, highlighting its effectiveness in cross-user applications.

Whether for the user-specific or user-independent scenario, the final performance evaluation is based on the average of the five cross-validation iterations. This approach not only helps to reduce the random errors caused by data partitioning but also provides more reliable and repeatable performance metrics. Through the above methods, the generalization ability and stability of the model are ensured in different scenarios, thereby laying a solid theoretical foundation for its practical application.

TABLE V
THE COMPARISON WITH OTHER REHABILITATION SYSTEMS

	DoF	Communication mode	Home-based/ Portability	Haptic feedback	sEMG-driven subject-independent
Yang et al. [4]	One	LAN	Yes	Yes	No
Liu et al. [5]	One	LAN	Yes	Yes	No
Patel et al. [12]	Six	LAN	No	Yes	No
Chen et al. [22]	Six	Bluetooth.	Yes	No	No
This study	Three	WAN	Yes	Yes	Yes

V. DISCUSSION

As shown in Table V, the proposed rehabilitation system offers several advantages over existing systems: Firstly, it incorporates a design with three DoFs, offering greater flexibility and adaptability compared to systems with only one DoF in previous studies. Secondly, the use of Wide Area Network (WAN) enables broader coverage and higher data transmission capacity compared to Local Area Networks (LANs) or Bluetooth-based solutions. Thirdly, the home-based nature of the system makes it suitable for deployment in home-based environments, significantly improving user convenience and accessibility. Additionally, the integration of haptic feedback plays a crucial role in enhancing user engagement and providing a more immersive rehabilitation experience. Finally, as an sEMG-driven system, it operates based on sEMG signals without requiring individualized calibration, thereby enhancing its generalizability and ease of use.

Telerehabilitation involves the use of internet technology to enable patients to access professional rehabilitation services remotely, without the need to visit a medical facility in person. Bilateral rehabilitation involves simultaneous training of both the affected and the unaffected limb of patients, aiming to promote neuroplasticity and enhance motor function recovery. By integrating these two approaches, a more flexible and efficient rehabilitation model can be developed, particularly benefiting stroke survivors and individuals requiring long-term rehabilitation support. Based on the above, a home-based dual-mode rehabilitation system using the upper limb exoskeleton is built. This system aims to integrate the advantages of telerehabilitation and bilateral rehabilitation to deliver efficient, convenient and personalized rehabilitation treatment for stroke patients. To validate the effectiveness of the telerehabilitation platform, experiments are conducted in three different locations: Beijing, Shenzhen and Takamatsu. Fig. 10 shows the motion trajectory and contact force variations at the slave side, indicating that the system can effectively transmit the therapist's direct operation and detect the contact force between the affected limb and the exoskeleton, even over long distances. Fig. 11 presents the AVE and STD of hourly communication delays recorded from 7:00 a.m. to 8:00 p.m. in histogram form, visualizing both the delay magnitudes and their variability across different locations.

Quantitative analysis presented in Table I further supports the above observation. Notably, the maximum communication delay across all locations remains below 300 ms [19], satisfying the real-time requirements of rehabilitation systems. It is worth noting that while the delay in Takamatsu is higher, it remains within an acceptable range and does not compromise the system's functional performance or clinical usability. In the control delay evaluation. Fig. 12 depicts the motion angle differences between the client PC and the microcontroller, while Table II provides detailed measurements of total delay, serial transmission delay and motion control delay under three different DoFs. The results show that the motion control delay accounts for most of the time, such as the motion control delay of 249 ms for the 5th DoF.

In the rehabilitation process, latency plays a crucial role. It not only affects the smoothness of interactions between users and therapists but also directly impacts the quality of rehabilitation outcomes. Firstly, in rehabilitation activities that require immediate feedback, any noticeable delay can undermine this immediacy, making it difficult for users to adjust their actions based on the feedback they receive. This is particularly true in training processes that utilize haptic feedback mechanisms, where latency can diminish the system's sense of immersion and the authenticity of the interaction, thereby reducing user engagement and satisfaction. Secondly, from a perspective of rehabilitation effectiveness, latency can significantly compromise the accuracy and efficacy of training. The real-time correction of erroneous movements is a critical component of rehabilitation training. Delays can lead to late corrections, further degrading the quality of rehabilitation even causing secondary injuries. Therefore, when designing rehabilitation solutions, minimizing latency and ensuring rapid response are especially important. Future directions include leveraging technologies such as edge computing, optimized data transmission methods and adaptive latency compensation to minimize latency. These approaches can provide more effective support for real-time feedback and interaction, thereby improving user experience and rehabilitation outcomes while ensuring safety and efficiency throughout the process.

In the bilateral rehabilitation, a dual-input CNN model is used to suppress both the intra-subject and inter-subject variability of sEMG signals during the continuous elbow movements. Furthermore, the user-dependent and user-independent predictions are realized. The five-fold cross-validation method ensures the reliability and repeatability of evaluation metrics and reduces random errors caused by data segmentation. The results demonstrate the effectiveness of the

This article has been accepted for publication in IEEE Journal of Biomedical and Health Informatics. This is the author's version which has not been fully edited and content may change prior to final publication. Citation information: DOI 10.1109/JBHI.2025.3588404

subject-independent prediction with the dual-input CNN model. The comparison of different methods' performance is recorded in Table VI. Compared with other methods, the R obtained by the proposed method is the highest (0.9926). The RMSE (5.83) obtained by the proposed method is the second lowest, just above the RMSE (4.07) reported by Sun et al. The method proposed by Sun et al. focuses on modeling for each subject, i.e., addressing intra-subject variability. In contrast, the method proposed in this study aims at multi-subject modeling, accounting for both intra-subject variability and inter-subject variability.

TABLE VI
THE COMPARISON WITH OTHER PREDICTION METHODS

	RMSE (°)	R
Yang et al. [20]	20.44	0.8940
Zhao et al. [21]	17.59	0.9100
Li et al. [6]	15.26	0.9290
Yang et al. [22]	13.668	0.8650
Yang et al. [16]	12.99	0.8840
Sun et al. [18]	4.07	0.9800
This study	**5.83**	**0.9926**

In summary, this study demonstrates that the tele-rehabilitation system can provide low-latency and stable communication services across various regions, while the prediction model based on the dual-input CNN can effectively deal with inter-subject variability. By integrating tele-training and bilateral training, a home-based rehabilitation system is constructed. This system-integrated rehabilitation solution not only overcomes geographical barriers by offering continuous and professional rehabilitation guidance to patients but also enhances potential value through several specific clinical application scenarios: (1) Community Health Centers: Patients at community health centers can access personalized rehabilitation training under the guidance of professional therapists via the tele-rehabilitation system. (2) Home-based Rehabilitation Environment: For patients with mobility limitations or those residing in remote areas, a home-based rehabilitation system is especially valuable, which enables individuals to perform rehabilitation exercises conveniently and safely at home. (3) Hospital Rehabilitation Departments: Within hospital rehabilitation departments, the tele-rehabilitation system serves as a complementary tool to traditional face-to-face therapy. It enables continuous post-discharge care, thereby helping to reduce readmission rates.

Despite the contributions of this study, two important limitations should be addressed in future research. Firstly, the relatively small sample size may increase the risk of sampling bias and limit the generalizability across diverse population characteristics. Therefore, although our preliminary results suggest the potential benefits of the proposed system, these findings require further validation in larger and more diverse cohorts to confirm their reliability and broad applicability. Secondly, this study has not yet been validated through clinical trials. While promising results are obtained in controlled laboratory settings, the reproducibility and real-world feasibility of these findings in clinical environments remain to be confirmed. The next step should involve designing and conducting rigorous clinical trials to rigorously assess the safety and efficacy of the proposed system across diverse patient populations. Additionally, future work could explore the integration of electrical stimulation, combining the movement-based rehabilitation with neuromuscular stimulation as complementary therapeutic strategies [23].

To further enhance the practical value of the system, more attention should be directed towards the user experience, particularly in terms of comfort and usability. Based on the preliminary user feedback, several key areas have been identified for improvement in future work: (1) Ergonomic Design Optimization: User feedback indicates that prolonged use of the current system may lead to physical discomfort. Future work will focus on refining the device's design to better conform to ergonomic standards and improve long-term wearability. (2) Simplifying Operation Processes: Although the current system's user interface is relatively intuitive, users still face a learning curve when operating some advanced features. Future iterations will aim to simplify operation workflows, develop more user-friendly interfaces, and provide detailed user guides. In summary, the continuous system improvement requires the establishment of an effective user feedback mechanism. Future work will not only focus on technological advancements but also involve regularly collecting user opinions to make corresponding adjustments.

VI. CONCLUSION

Focused on robot-assisted rehabilitation for individuals with upper limb hemiplegia, a dual-mode rehabilitation system is proposed, including the therapist-in-the-loop tele-training based on a cloud server and the bilateral training based on sEMG and IMU signals. Tele-rehabilitation can expand the coverage of training, provide professional guidance and enhance convenience. The feasibility of the tele-rehabilitation system is verified through experiments conducted across three different regions. In the bilateral training, the subject-independent prediction of continuous movements is realized through a dual-input network based on sEMG and IMU. This approach improves prediction accuracy of motion intention while also considering the naturalness of human–robot interaction. The dual-mode rehabilitation system based on tele-training and bilateral training realizes the combination of therapist guidance and self-training, which is of great significance for home-based rehabilitation of stroke patients.

REFERENCES

[1] S. S. Martin et al., "2024 Heart Disease and Stroke Statistics: A Report of US and Global Data From the American Heart Association," Circulation, vol. 149, no. 8, pp. e347-e913, Jan. 2024, doi: 10.1161/CIR.0000000000001209.

[2] K. Roesner, B. Scheffler, M. Kaehler, B. Schmidt-Maciejewski, T. Boettger and S. Saal, "Effects of physical therapy modalities for motor function, functional recovery, and post-stroke complications in patients with severe stroke: a systematic review update," Syst. Rev. 13, no. 270,

Oct. 2024, doi: 10.1186/s13643-024-02676-0.

[3] X. Li, Y. He, D. Wang and M. J. Rezaei, "Stroke rehabilitation: from diagnosis to therapy," Front. Neurol., vol. 15:1402729, Aug. 2024, doi: 10.3389/fneur.2024.1402729.

[4] Z. Yang, S. Guo, L. Ren, R. An, Y. Liu and M. Kawanishi, "S2-RTPIC: A State-Switching Remote Therapist Patient Interaction Control for Telerehabilitation," IEEE Trans. Industr. Inform., vol. 21, no. 1, pp. 366-375, Jan. 2025, doi: 10.1109/TII.2024.3452244.

[5] Y. Liu, S. Guo, Z. Yang, H. Hirata and T. Tamiya, "A Home-based Tele-rehabilitation System With Enhanced Therapist-patient Remote Interaction: A Feasibility Study," IEEE J. Biomed. Health. Inform., vol. 26, no. 8, pp. 4176-4186, Aug. 2022, doi: 10.1109/JBHI.2022.3176276.

[6] H. Li, S. Guo, D. Bu, H. Wang and M. Kawanishi, "Subject-Independent Estimation of Continuous Movements Using CNN-LSTM for a Home-Based Upper Limb Rehabilitation System," IEEE Robot. Autom. Lett., vol. 8, no. 10, pp. 6403-6410, Oct. 2023, doi: 10.1109/LRA.2023.3303701.

[7] Y. Liu, S. Guo, Z. Yang, H. Hirata and T. Tamiya, "A Home-Based Bilateral Rehabilitation System With sEMG-based Real-Time Variable Stiffness," IEEE J. Biomed. Health. Inform., vol. 25, no. 5, pp. 1529-1541, May 2021, doi: 10.1109/JBHI.2020.3027303.

[8] E. Zasadzka et al., "Application of an EMG-Rehabilitation Robot in Patients with Post-Coronavirus Fatigue Syndrome (COVID-19)-A Feasibility Study," Int. J. Environ. Res. Public Health., vol. 19, no. 16, Jun. 2022, Art. no. 10398, doi: 10.3390/ijerph191610398.

[9] C. Lambelet, M. Lyu, D. Woolley, R. Gassert and N. Wenderoth, "The eWrist — A wearable wrist exoskeleton with sEMG-based force control for stroke rehabilitation," 2017 International Conference on Rehabilitation Robotics (ICORR), London, UK, Jul. 2017, pp. 726-733, doi: 10.1109/ICORR.2017.8009334.

[10] C. Lambelet, et al., "Characterization and wearability evaluation of a fully portable wrist exoskeleton for unsupervised training after stroke", J. Neuroeng. Rehabilitation, vol. 17, no. 1, Oct. 2020, Art. no. 132, doi: 10.1186/s12984-020-00749-4.

[11] D. Shi, W. Zhang and X. Ding, "A Review on Lower Limb Rehabilitation Exoskeleton Robots," Chin. J. Mech. Eng., vol. 32, no. 74, Aug. 2019, Art. no. 2019, doi: 10.1186/s10033-019-0389-8.

[12] S. Atashzar, M. Shahbazi, M. Tavakoli and R. Patel, "A Computational-Model-Based Study of Supervised Haptics-Enabled Therapist-in-the-Loop Training for Upper-Limb Poststroke Robotic Rehabilitation," IEEE ASME Trans. Mechatron., vol. 23, no. 2, pp. 563-574, Apr. 2018, doi: 10.1109/TMECH.2018.2806918.

[13] J. Bai, A. Song, and H. Li, "Design and Analysis of Cloud Upper Limb Rehabilitation System Based on Motion Tracking for Post-Stroke Patients," Appl. Sci. vol. 9, no. 8, Apr. 2019, Art. no. 1620, doi:10.3390/app9081620

[14] Y. Chen, Z. Yang, and Y. Wen, "A Soft Exoskeleton Glove for Hand Bilateral Training via Surface EMG," Sensors, vol. 21, no. 2, Jan. 2021, Art. no. 578, doi: 10.3390/s21020578.

[15] J. Li et al., "Motion intention prediction of upper limb in stroke survivors using sEMG signal and attention mechanism," Biomed. Signal Process Control, vol. 78, Sep. 2022, Art no. 103981, doi: 10.1016/j.bspc.2022.103981.

[16] X. Yang, F. Li, F. Hu, and W. Zhang, "Human Motion Estimation Based on EMG-Inertial Fusion:A Gaussian Filtering Network Approach," Acta Anat. Sin., vol. 5, pp. 991-1000, May 2024, doi: 10.16383/j.aas.c230581.

[17] F. Stival, S. Michieletto and A. De Agnoi and E. Pagello, "Toward a Better Robotic Hand Prosthesis Control: Using EMG and IMU Features for a Subject-Independent Multi Joint Regression Model," 2018 7th Biorob, Enschede, Netherlands, 2018, pp. 185-192, doi: 10.1109/BIOROB.2018.8487188.

[18] N. Sun, et al., "Continuous Estimation of Human Knee Joint Angles by Fusing Kinematic and Myoelectric Signals," IEEE Trans. Neural Networks Learn. Syst., vol. 30, pp. 2446-2455, Aug. 2022, doi: 10.1109/TNSRE.2022.3200485.

[19] U. Côté-Allard, C. L. Fall, A. Drouin, A. C. Lecours, C. Gosselin and K. Glette, "Deep Learning for Electromyographic Hand Gesture Signal Classification Using Transfer Learning," IEEE Trans. Neural Syst. Rehabilitation Eng, vol. 27, no. 4, pp. 760-771, Apr. 2019, doi: 10.1109/TNSRE.2019.2896269.

[20] Z. Yang, S. Guo, Y. Liu, H. Hirata, and T. Tamiya, "An intention-based online bilateral training system for upper limb motor rehabilitation," Microsyst. Technol., vol. 27, pp. 211–222, Jun, 2021, doi: 10.1007/s00542-020-04939-x.

[21] Y. Zhao, Z. Zhang, Z. Li, and Z. Yang, A. A. Dehghani-Sanij and S. Xie, "An EMG-Driven Musculoskeletal Model for Estimating Continuous Wrist Motion," IEEE Trans. Neural Syst. Rehabilitation Eng., vol. 28, no. 12, pp. 3113-3120, Dec. 2020, doi: 10.1109/TNSRE.2020.3038051.

[22] X. S. Yang, X. E. Wang, P. J. Wang and W. A. Zhang, "Estimation of human limb motion based on progressive unscented Kalman filter network," Acta Automatica Sinica, vol. 49, no. 8, pp. 1723−1731, Jul. 2024, doi: 10.16383/j.aas.c220523.

[23] Y. Bouteraa, I. B. Abdallah and A. Elmogy, "Design and control of an exoskeleton robot with EMG-driven electrical stimulation for upper limb rehabilitation", Ind. Robot, vol. 47, no. 4, pp. 489-501, May 2020, doi: 10.1108/IR-02-2020-0041.

He Li (Student Member, IEEE) received the M.S. degree in the School of Precision Instrument and Opto-Electronics Engineering from Tianjin University, Tianjin, China, in 2021. She is currently pursuing the Ph.D. degree at Beijing Institute of Technology, Beijing, China.

She has published 9 journal and conference papers. She researches the upper limb rehabilitation exoskeleton, sEMG signal processing, multi-sensor fusion, and telerehabilitation systems.

Shuxiang Guo (Fellow, IEEE) received the Ph.D. degree in mechanoinformatics and systems from Nagoya University, Nagoya, Japan, in 1995.

He is currently a Full Professor at the Department of Electronic and Electrical Engineering, Southern University of Science and Technology, Shenzhen, Guangdong, China. He is also a Chair Professor with School of Life Science, Beijing Institute of Technology, Beijing, China.

He has published about 500 refereed journal and conference papers. His current research includes biomimetic underwater robots, medical robot systems for minimal invasive surgery, microcatheter systems, micropumps, and smart materials (SMA, IPMC) based on actuators. Prof. Guo is the Editor-in-Chief for the International Journal of Mechatronics and Automation.

Ruijie He (Student Member, IEEE) received the B.S. degree from Northeastern University, Liaoning, China, in 2021. He is currently studying for his M.S. degree at Beijing Institute of Technology, Beijing, China.

He researches exoskeleton rehabilitation robotic systems and sEMG signal processing for biomedical applications.

Wang Bin, a director of the Interventional Vascular Department at the Aerospace Center Hospital, a leader in the sub discipline of peripheral vascular disease intervention, chief physician, and master's supervisor.

He is proficient in the interventional treatment of deep vein thrombosis and pulmonary embolism in the lower limbs, interventional treatment of acute and chronic ischemic peripheral vascular diseases, interventional embolization treatment of various hemorrhagic diseases, etc.

Mingchao Ding received the M.S. degree in imaging and nuclear medicine from Peking University School of Medicine in 2011. He is currently the president, chief physician, professor, and doctoral supervisor of the Aerospace Center Hospital, and the head of the Continuing Education and Training Base for Peripheral Vascular Interventional Physicians of the National Health Commission.

His current research includes endovascular treatment and emergency interventional treatment of ischemic peripheral vascular diseases, bleeding diseases, and thrombotic diseases.